Metastable phase-separated droplet generation and long-time DNA enrichment by laser-induced Soret effect

Mika Kobayashi*, Yoshihiro Minagawa, and Hiroyuki Noji*

Department of Applied Chemistry, Graduate School of Engineering University of Tokyo, Tokyo 113-8656, Japan

(Dated: October 23, 2024)

*Corresponding author. E-mail: kobayashi.phys@gmail.com; hnoji@g.ecc.u-tokyo.ac.jp

Abstract

Spatiotemporally controlled laser-induced phase separation (LIPS) offers unique research avenues and has potential for biological and biomedical applications. However, LIPS conditions often have drawbacks for practical use. For instance, LIPS droplets are unstable and diminish after the laser is terminated, which limits their applications. In this study, we developed a novel LIPS method using the laser-induced Soret effect to generate phase-separated droplets at the laser spot in an aqueous two-phase system (ATPS) of dextran (DEX) and polyethylene glycol (PEG). When DEX-rich droplets were generated in the DEX/PEG mix of which concentrations are on the coexisting curve, the droplets showed unprecedently high longevity; the DEX droplets were retained over 48 h. Although the mechanism underlying this counterintuitive phenomenon is unclear, this observation suggests that there is an unknown metastable state. By exploiting the capability of DEX-rich droplets to enrich nucleic acid polymers, we achieved stable DNA enrichment in LIPS DEX droplets with a high enrichment factor of 1400 ± 400. Further, we patterned DNA-carrying DEX-rich droplets into a designed structure to demonstrate the stability and spatiotemporal controllability of DEX-rich droplet formation. This is the first LIPS droplet generation in a DEX/PEG system with flexible conditions for the usage of LIPS droplets and opens new venues for the biological and medical applications of LIPS.

Keywords: laser induced phase separation, LLPS, droplet kinetics, DNA enrichment

Liquid-liquid phase separation (LLPS) attracts large interests in biological sciences since the recent findings that phase separation plays important roles in a wide variety of biomolecular systems[1–4]. In addition to biological droplets, the ATPS (aqueous two-phase system) of Dextran (DEX) and polyethylene glycol (PEG) also draws a large attention because ATPS of DEX/PEG can enrich some of biomolecules in DEX-rich phase[5–8] while these polymers are chemically and biologically inert and thereby they show fine biocompatibility. In particular, DEX-rich droplets in DEX/PEG ATPS have been reported to well enrich DNA molecules[9]. Other biomolecules such as RNA and proteins are also reported to have enriched in the DEX-rich phase[10,11]. For these reasons, DEX/PEG ATPS was utilized in microchemical/biological systems for efficient DNA and protein enrichment[8,12] or in artificial cell models to enrich biomolecules and/or enhance biomolecular reactions[11,13–15]. Thus, spatiotemporal control of LLPS including DEX/PEG ATPS under the microscope is of great importance for biological applications.

Laser-induced phase separation (LIPS) is a method to generate LLPS droplets in a controlled manner and it has been investigated in several systems[16–27]. Local heating upon laser irradiation to LCST (lower critical solution temperature) systems is a simple LIPS method[19] where droplets are created when the heated region satisfies the two-phase condition. However, the generation temperature for the LIPS in LCST systems is limited by the phase diagram and generally it requires high generation temperature which is not applicable in biological experiments. Especially, it is difficult to keep precise temperature control for biological reactions. In the case of DEX/PEG systems, there are some systems which show LCST[28]. In principle, LIPS in those systems should be possible but LIPS DEX droplet generation has never been reported so far. This would be partly because of the above reasons.

Another approach for LIPS is to use the Soret effect (thermophoresis), which is a non-equilibrium phenomenon wherein a concentration gradient is formed under a temperature gradient[29]. In this case, local concentration is modulated by temperature gradient, but temperature does not directly drive

phase separation. This means that the generation temperature is basically not limited by the phase diagram. LIPS by the Soret effect can be conducted at a desired temperature if the appropriate concentration gradient is formed. The concentration gradient of a molecule induced by the Soret effect, ∇c, is described as

$$\nabla c = -S_T\, c(1 - c)\, \nabla T,$$

where c, ∇T, and S_T represent the molecular fraction, temperature gradient, and ratio of the thermal mass diffusion coefficient (D_T) to the mutual mass diffusion coefficient (D), respectively; $S_T = D_T/D$. The value of S_T ranges from 10^{-5} to 10^{-1} [30]. Whether a molecule accumulates ($S_T < 0$) or is excluded ($S_T > 0$) along a temperature gradient depends on its species and its combination with other molecules in the mixture[31]. On the other hand, the concentration gradient generated by the Soret effect is generally not sufficient to induce phase separation. There are, therefore, only a few reports on LIPS using the Soret effect. Delville et al. demonstrated LIPS in a quaternary micellar system because the required concentration change was sufficiently small to achieve phase separation[16,17]. Voit et al. studied thermal patterning on a polymer blend using a focused laser beam and modulated phase separation near the critical point where the Soret coefficient diverges[21,22].

Another drawback of LIPS so far is that LIPS droplets prepared using these methods are ephemeral and disappear after the termination of laser irradiation because the droplets are formed under non-equilibrium conditions in a stable single phase. The duration of the LIPS droplets is basically determined by the diffusion of molecules. In previous reports on LIPS experiments with binary mixtures, LIPS droplets disappeared within tens of minutes[21,25]. Thus, LIPS droplets are principally unstable and revert to the miscible solution state after laser induction[21,25], which limits its range of application.

In this study, we aimed to develop a novel LIPS methodology for the generation of phase-separated DEX-rich droplets in a DEX/PEG system by use of the laser-induced Soret effect. DEX has a unique feature; this polymer exhibits a negative Soret coefficient, $S_T < 0$[31]; DEX molecules accumulate to

the hot region along the temperature gradient. Thus, the negative S_T of DEX is, in principle, suitable for LIPS with the Soret effect. We developed a local heating system in which an infrared laser spot was introduced on a coverslip coated with a semiconductor which absorbs the infrared light and produces heat. The local heating produced a temperature gradient, which resulted in the local condensation of DEX via the Soret effect. The laser-induced Soret effect successfully triggered the formation of DEX-rich droplets. We discovered that the generated droplets were extraordinarily stable; the droplets were retained for over 48 h. It was also found that the DEX-rich droplets enriched DNA molecules by a factor of 1400. Finally, we demonstrated the patterning of DNA-containing droplets along the defined structures, by exploiting the controllability, longevity and capability for DNA enrichment of the LIPS-induced DEX-rich droplet.

LIPS droplet generation by laser-induced Soret effect

We produced LIPS droplets in a miscible mixture of DEX ($Mw = 4.5\text{–}6.5 \times 10^5$) and PEG ($Mw = 3.5 \times 10^4$). A phase diagram of the DEX/PEG system is illustrated in Fig. 1a. It does not change within the experimental temperature range of 293–363 K. Therefore, heating by laser irradiation did not directly affect the phase of the DEX/PEG system (See Methods). We performed experiments on a DEX/PEG mix on the coexisting curve, which is the phase boundary between single- and two-phase states, with the expectation that the system would inevitably enter the two-phase region by the small change in concentration induced by the Soret effect. The DEX/PEG mixture on the coexisting curve was prepared experimentally as follows; at first, a DEX/PEG was prepared at an initial composition in the two-phase region —DEX at 6 wt.% and PEG at 2.6 wt.% (open circles in Fig. 1a). The DEX/PEG mixture was equilibrated to form macroscopic two phases and complete phase separation, as shown in the photograph in Fig. 1a. Each phase obtained by the preparation should be exactly on the phase boundary because it is an equilibrium phase. The DEX/PEG compositions of the upper PEG-rich phase and the lower DEX-rich phase are estimated from the

101 fluorescent intensity of the spiked, fluorescently labelled DEX and PEG (Fig. 1a), respectively. The
102 compositions were consistent with those reported in a previous study[32]. The upper PEG-rich phase
103 solution was used in subsequent experiments to induce DEX-rich droplet generation by LIPS.

104 Local heating was performed under a microscope using an infrared (IR) laser. Figure 1b illustrates
105 a schematic of the experimental setup. A temperature gradient was generated at the laser focus point,
106 where the IR laser light was absorbed by the ITO coat on a coverslip of a sample cell. The schematic
107 of DEX-rich droplet generation by LIPS is shown in Fig. 1c. The temperature gradient produced upon
108 the laser irradiation attracts DEX molecules via the Soret effect. The temperature at the heating spot
109 during laser irradiation was estimated to be +10 K from the surrounding medium, generating a
110 temperature gradient of 0.1 K/μm (Supplementary Note 1). Subsequently, a DEX-rich droplet phase
111 appeared at the focal point of the IR laser.

112 Figure 1d illustrates time-lapsed images of the droplet-generation process (See also
113 Supplementary Video 1). When the laser irradiation was initiated, the growth of the dark domain in
114 the phase contrast images was observed, as well as the growth of a fluorescence spot in the
115 fluorescence images. After the irradiation time for 10 min, the laser was switched off. Then, the small
116 droplets suddenly appeared around the main droplet (see phase-contrast images at 10 or 60 s after
117 laser termination in Fig. 1d). These satellite droplets gradually coalesced into the main droplet. The
118 droplet interface was not clear during laser irradiation, and it became sharp after laser termination. It
119 is likely that the active mass transport of DEX by the laser-induced Soret effect perturbed the
120 formation of a stable interface. We also examined LIPS using an ITO-free glass substrate. DEX
121 accumulation and droplet formation were not observed (Supplementary Note 2), confirming that
122 droplet generation was not induced by the radiation pressure or electromagnetic force of the laser, but
123 by local heating, which caused the Soret effect. We confirmed that the temperature of the generated
124 droplet can be changed after the laser is switched off (Supplementary Note 3).

125 When the DEX/PEG mix was prepared at concentrations below the coexisting curve (blue circle

126 in the phase diagram in Fig. 1a), laser irradiation failed to form a droplet, although DEX condensed
127 (Fig. 1e). When the irradiation was terminated, the accumulated DEX molecules diffused within
128 minutes. This means we need an initial sample very close to the coexisting curve for LIPS using the
129 Soret effect as more investigated below.
130

131 **Longevity of LIPS droplet**

132 The generated DEX droplets exhibited remarkable longevity. Figure 2a shows a representative
133 series of time lapsed images for 2 days. Figure 2b exhibits the time course of the diameter of the
134 droplet shown in Fig. 2a. Initially, the diameter was approximately 7 μm. After the initial shrinkage
135 process of 1–2 h, the droplet size reached a steady value of approximately 3 μm. Figure 2c illustrates
136 the diameters of the droplets generated under the same experimental condition plotted as a function
137 of the laser irradiation time t_{IR}. The initial diameter ranged from 6–12 μm, and the final diameter was
138 1–3 μm. Neither the initial nor the final diameter did not show a clear t_{IR}-dependence. This suggests
139 that DEX condensation by the laser-induced Soret effect plateaued within 5 min of irradiation.

140 We investigated the relationship between the droplet longevity and the initial composition of
141 DEX/PEG mixture. In particular, we asked how stable the generated droplets are when the initial
142 concentrations of DEX and PEG are below the coexisting curve (inset of Fig. 2d). For this purpose,
143 we prepared DEX/PEG mixtures by diluting the PEG-rich phase taken from DEX/PEG ATPS
144 solution, which systematically changed the distance from the coexisting curve (inset of Fig 2d). When
145 the DEX/PEG mix was prepared at a dilution factor of 0.9 (pink triangle in the inset of Fig. 2d), LIPS
146 droplets were once generated, however, they disappeared within 30 min (pink triangles in Fig. 2d).
147 The droplets prepared in diluted mix shrank significantly faster than that without dilution. When the
148 DEX/PEG mix was more diluted; the dilution factor was less than 0.9 (blue crosses in the inset of
149 Fig. 2d), and no droplet formation was observed. Figure 2e shows the time-courses of the droplet
150 diameter for the samples with the dilution factors from 1 and 0.9. We analysed the initial linear regime

151 using linear fitting to estimate the initial speed of droplet shrinkage, v_0. The results are shown in Fig.
152 2f. The rate of shrinkage, v_0 decreases systematically as the dilution factor approaches 1 (no dilution:
153 on the coexisting curve). This suggests that the driving force to revert the droplet to the original
154 miscible state decreases, when the composition of DEX/PEG mix approaches the coexisting curve.
155 The relationship between the initial composition in the phase diagram and the appearance of longevity
156 is schematically explained in Fig. 2 g and h. These findings confirm that the DEX/PEG mix
157 composition has to be quite close or on the coexisting curve for stable DEX droplet generation.
158
159
160 **DNA enrichment in LIPS droplet**
161 We attempted DNA enrichment in LIPS DEX droplets by exploiting the capability of DEX-rich
162 droplets to enrich DNA molecules[9]. The concept of our experiment is schematically illustrated in Fig.
163 3a; the longevity of DEX-rich LIPS droplets is expected to achieve stable DNA enrichment. First, we
164 examined the possibility of DNA enrichment in LIPS droplets. The PEG-rich phase solution for LIPS
165 was prepared with λ-DNA (48,502 bps) through the protocol as same as the above experiments. The
166 DNA concentration in the prepared PEG-rich solution was 70 pg/μL (see Methods and
167 Supplementary Note 4). We conducted LIPS with DNA-containing PEG-rich solution as same as
168 above. Fig. 3b shows the images of a LIPS DEX droplet generated upon laser irradiation for 5 min.
169 The fluorescence image of the DNA intercalator reveals the enrichment of DNA in the LIPS droplet.
170 The droplets with enriched DNA were as stable as droplets prepared without DNA. After initial
171 shrinkage, the droplets retained a constant diameter over 24 h. The fluorescence signal from DNA
172 was more stable than that from DEX; the fluorescence signal of DNA in droplets was observed even
173 after 18 h (Fig. 3c), while the fluorescence signal of DEX became significantly darker compared with
174 the initial fluorescence signal (t = 0 h).
175 For more quantitative analysis on the concentration of DNA and DEX of the LIPS droplets, the

176 fluorescence intensity of the droplets was measured with confocal microscopy. This is because the
177 fluorescence images of the droplets in epifluorescence microscopy contained a considerable level of
178 background fluorescence intensity from the surrounding medium, hampering accurate measurement.
179 LIPS droplets were prepared on laser-equipped epifluorescence microscopy and subsequently
180 translated to confocal microscopy for time-evolution observation. Therefore, the confocal microscopy
181 observations were started several minutes after LIPS. However, as shown below, the time evolution
182 of the fluorescent signal of DNA/DEX in LIPS droplets exhibited significantly slower change, in the
183 order of tens of minutes. Thus, the delay caused by sample translation was neglected.

184 Figure 4a displays the representative time-lapsed images of the LIPS droplets visualized by
185 fluorescent DNA/DEX after laser irradiation for 12 min. The time course of droplet diameter is shown
186 in Extended Data Fig. 1a. It showed an exponential decay and converged to a finite value around 3
187 μm. The fluorescent intensity of DNA in the LIPS droplet showed a temporal rise around 51 min,
188 followed by decay. In contrast, the fluorescence intensity of DEX showed a simple monotonous decay.
189 We defined the enrichment factor of DNA, EF^{DNA} as the ratio of DNA concentration in a LIPS droplet
190 to that in the surrounding PEG-rich solution, $EF^{\mathrm{DNA}} = [\mathrm{DNA}]_{\mathrm{droplet}}/[\mathrm{DNA}]_{\mathrm{surrounding}}$. The DNA
191 concentration in droplets ranged from 50 to 200 ng/μL, while that of the surrounding PEG-rich phase
192 solution was 70 ± 10 pg/μL (see Methods and Supplementary Note 4). The time evolution of EF^{DNA}
193 is illustrated in Fig. 4b. As observed in the time-lapsed images, EF^{DNA} initially showed a transient
194 rise to the maximum value around 50 min, followed by slow decay to a steady level. The statistical
195 analysis showed the mean values of the initial, maximum, and steady stages were 1200, 2000, 1400
196 (Fig. 4d). The individual data were plotted against the initial droplet diameter d_0 in Extended Data
197 Fig. 2a. Although the exact mechanism for the transient rise of EF^{DNA} is not clear, it is attributable to
198 condensation upon the droplet shrinkage (See Extended Data Fig. 1a). Time $t_{\max}$ when EF^{DNA} showed
199 its maximum is shown in Extended Data Fig. 3a. In some cases, there was no evident maxima
200 (Extended Data Fig. 3b).

201 The concentration ratio of DEX of the droplet to the surrounding solution, CR^{DEX} was estimated
202 as the fluorescence intensity ratio of the droplet to that in the surrounding PEG-rich solution, CR^{DEX}
203 = $[DEX]_{droplet}/[DEX]_{surrounding}$ (Supplementary Note 4). Fig. 4c shows the time evolution of CR^{DEX}
204 that exhibited an exponential decay from approximately 6 to a plateau level, around 2 (Fig. 4c). The
205 trend of the DEX concentration decrease can be seen in the result of statistical analysis shown in Fig.
206 4e. The validity of the change is discussed in Supplementary Note 5. The individual data were plotted
207 against the initial droplet diameter d_0 in Extended Data Fig. 2b. The timescale of the decay in CR^{DEX}
208 was similar to that of the diameter (Extended Data Fig. 4).
209 The presence of DNA did not show a significant effect on the behaviour of the LIPS droplets. The
210 decay rate of the droplet diameter was the order of 10^1 min in both cases, w/ and w/o DNA (Extended
211 Data Fig. 1b). The initial value and the final value of CR^{DEX} were almost the same between w/ and
212 w/o DNA shown in Fig. 4e.
213
214 **Comparison of LIPS droplet and spontaneous droplet**
215 We compared LIPS droplets with droplets formed by spontaneous phase separation. The
216 spontaneous droplets of the DEX-rich phase were prepared by agitation of the two-phase DEX/PEG
217 mix which is the same composition as that used in LIPS experiments and observed in confocal
218 microscopy (Supplementary Note 6). The DNA enrichment factor EF^{DNA} and the DEX concentration
219 ratio CR^{DEX} of spontaneous droplets were compared with those of LIPS droplets in Figs. 5a and 5b,
220 respectively. The mean values of initial or final EF^{DNA} for LIPS droplets are 1200 and 1400 which
221 are higher than EF^{DNA} for spontaneous droplets, around 600 (Fig.5a). The distribution of EF^{DNA} for
222 LIPS droplets is wider than that of spontaneous ones. The mean values of initial or final CR^{DEX} for
223 LIPS droplets are 6.9 and 3.0 which are smaller than CR^{DEX} of spontaneous ones, 9.4 (Fig.5b).
224 For the direct comparison of LIPS droplets and spontaneous droplets, we conducted LIPS with
225 ATPS of DEX/PEG; the PEG-rich phase solution containing spontaneous DEX-rich droplets (Fig.

226 5c-f). LIPS droplets were generated as same as in the other experiments. The fluorescent intensity of
227 DNA in the LIPS droplet at $t = 7$ min after generation was higher than the spontaneous one by a factor
228 of 4.3. The intensity of DEX was lower than the spontaneous one by a factor of 0.7. Thus, the direct
229 comparison confirmed that LIPS droplets have higher EF^{DNA} and lower CR^{DEX} than those of
230 spontaneous droplets. These observations indicate that the property of LIPS droplets is not very far
231 from that of spontaneous phase separation, but different from it. In the PEG concentration in this
232 study, the Soret effect of DNA itself could contribute to the mechanism for the higher EF^{DNA} for LIPS
233 droplets than that of spontaneous one[33,34]. If so, EF^{DNA} could increase further by increasing t_{IR} up to
234 the equilibrium of the Soret effect. Braun et al. demonstrated laser-induced DNA enrichment using
235 the Soret effect and convection although it is not a phase separating system[35]. The enriched DNA in
236 their method diffused away after heating. In our case, convection is negligible since local heating is
237 achieved by heating the ITO surface at the bottom of the sample cell. Note that we confirmed that the
238 Soret effect of DNA itself is not the mechanism for the stable DNA enrichment in LIPS droplets
239 (Supplementary Note 7).
240

241 **Composition of LIPS droplet**

242 The composition of LIPS droplets was estimated in confocal measurements by spiking
243 fluorescently labelled DEX and PEG in DEX/PEG mix (See Methods and Extended Data Fig. 5). The
244 initial and final DEX/PEG compositions of LIPS are plotted as the dotted and closed blue circles in
245 Extended Data Fig. 5d, respectively. These compositions were estimated from the mean values of
246 CR^{DEX} and CR^{PEG} at the initial state, i.e., just after LIPS: $t \sim 5$ min and after long-time incubation: $t \sim$
247 100 min (Extended Data Fig. 5a, b, c). The initial composition is close to the composition of the DEX-
248 rich phase in the spontaneous ATPS of DEX/PEG (red triangle in Extended Dana Fig. 5d), while the
249 final composition is close to the PEG-rich phase (red circle in Extended Dana Fig. 5d). This means
250 that the DEX/PEG composition of LIPS droplet gradually changes with time, approaching to the

251 composition of PEG-rich phase. However, as seen in the stable plateau of CR^{DEX} in Fig. 4c, the LIPS
252 droplet almost pauses the composition change to stay at a particular composition in the metastable
253 state.
254
255 **Patterning of LIPS droplets**
256 Finally, we attempted to demonstrate the controllability, reproducibility, and longevity of LIPS
257 droplets by patterning LIPS droplets in the presence of DNA along a designated structure. Multiple
258 LIPS droplets were generated at the defined position to draw a heart mark by laser irradiation for 5
259 min (Supplementary Video 2). The time interval between each LIPS was 1 min and the distance
260 between droplets was approximately 50 μm. Fig. 6 shows the fluorescence image of DNA-containing
261 LIPS droplets, stained with the intercalator dye. The patterned LIPS droplets demonstrate not only
262 the controllability of LIPS but also that LIPS droplets do not interfere with the formation of neighbour
263 droplets under the present condition. More complicated patterning should be easily possible if our
264 method is combined with laser foci technique[36]. In preliminary experiments, we also found that it is
265 possible to translocate LIPS droplets by moving the laser focal point. Exploiting these phenomena,
266 the coalescence of two droplets was also demonstrated via manipulation (Supplementary Video 3).
267 This demonstration confirms the fluidity of the LIPS droplets, stating that the longevity is not caused
268 by trivial processes such as gelation or other chemical reactions. We also observe the abrupt
269 disappearance of LIPS droplets by short laser irradiation (Supplementary Video 4). Thus, the current
270 system allows for the microscopic handling of LIPS droplets: the patterning, translocation, fusion,
271 and clearance of the DEX-rich droplets, although the precise understanding of the mechanism for
272 these phenomena needs further studies.
273
274 **Discussion**
275 The most prominent finding of this study is the extraordinarily long-time stability of the LIPS

droplets which allows stable DNA enrichment. The generated droplets in our method are principally non-equilibrium droplets because the initial state of the sample is a homogeneous single PEG-rich phase. Intuitively, the droplets were expected to disappear, as observed in the LIPS experiments conducted thus far[21,25]. However, the generated droplets did not vanish for a significantly long time after the laser was disabled. We observed a distinct decrease in the diameter, indicating that the system moved towards the original point on the coexisting curve. However, the shrinkage stopped at a point before returning to the original homogenous PEG-rich phase. Resultantly, the DEX/PEG composition of the droplets was close to but not exactly on the phase boundary (Extended Data Fig. 5). These observations mean that LIPS droplets were stacked in a metastable state. The stable LIPS droplets were also generated by using ATPS of DEX/PEG with different compositions, suggesting the generality of the stable LIPS droplets. Regarding the metastability, it is also worth noting the laser-induced disappearance of LIPS droplets (Supplementary Video 4). The laser irradiation seems to work as a perturbation to agitate the metastable droplets and the surrounding phase, and as a result, the droplets returned into the most stable state of the homogeneous phase. Consistent with this interpretation, spontaneously formed DEX-rich droplets in DEX/PEG ATPS which are stable in nature were retained even after the laser irradiation (Supplementary Video 5).

The initial condition of the sample on the phase boundary would be a key to the mechanism for the longevity of LIPS droplets. For the system exactly on the phase boundary, the other coexisting phase is energetically the same. This implies that, in principle, the system can shift towards both directions. This can be a similar situation to the coexistence of the ice at 0 °C in water at 0 °C. There should be competing effects between two equilibrium phases to which the system should go. The initial speed of droplet shrinkage decreased when the system was approaching the coexisting curve (Fig. 2f), suggesting that the driving force to cross the phase boundary to return toward the original equilibrium in the one-phase region dramatically decreases and this causes the longevity as schematically illustrated in Fig. 2g and h. On the other hand, this contention does not give full

301 explanation for the reason why the system has metastable states.

302 The present study indicates that there is an unknown mechanism which prevents the system from
303 crossing the phase boundary to return to the one-phase region. According to the classical nucleation
304 theory for phase separation, there is a critical radius R_c for droplet growth, for which the energy barrier
305 is determined by the interfacial energy and the bulk free energy of a droplet. While droplets of radius
306 smaller than R_c preferentially shrink, droplets show a stable growth when they occasionally reached
307 R_c[37]. In the reverse process, it should be different from the same R_c but there would be a similar energy
308 barrier for droplet shrinkage when the system crosses the phase boundary from the two-phase region.
309 That might be a mechanism for the remarkable longevity of the LIPS droplets. Of course, this model
310 would be too simplified. The exact understanding of the molecular mechanism for the metastability
311 of LIPS droplets needs future study.

312 In recent years, many studies reported that intracellular droplets of biomolecules, termed 'cell
313 biological droplets' play pivotal roles in biology[1–3,38–40]. Thereby, the physicochemistry of phase
314 separation systems attracts large attention not only in soft matter physics but also in chemical biology,
315 biophysics and molecular biology. It would be interesting to apply our method to systems consisting
316 of cell extract or living cell systems. The DEX/PEG system investigated herein also attracts attention
317 because the DEX-rich droplet is a model system to build protocell or artificial cell systems[6]. Our
318 method can be utilized to produce cellular structures in artificial cells, or to the local formation of
319 DNA origami structures. So far, we cannot keep both the LIPS droplet and the surrounding phase at
320 the same temperature in principle, but the present method enables us to do it. Our method has no
321 limitation in generation temperature and the temperature can be changed even after generation
322 (Supplementary Note 3), which provides a way to develop new tools for biochemical reactions and
323 digital bioassays such as digital PCR. Further, the PEG-rich phase enables the enrichment of rare
324 substances and their manipulation from its dilute solution, which could be applied to drug delivery.
325 We preliminarily confirmed that RNA could also be enriched in the LIPS droplets. Proteins such as

326 antibodies can be enriched in DEX-rich droplets, in particular when they are tagged with dextran-
327 binding domain (DBD)[8]. Considering these, the present LIPS method would be a technological basis
328 for the microscopic manipulation of biological molecules/systems by use of LIPS droplets as a carrier.
329 In summary, we succeeded in metastable LIPS droplet generation with unexpected longevity
330 which has never been observed before. The counterintuitive longevity is putting a fundamental
331 question to physics. It is also the first report of success in LIPS DEX droplet generation using the
332 DEX/PEG system and in LIPS DNA droplet generation which keeps fluidity. We achieved highly
333 stable DNA enrichment by a factor of thousands. The advantage of our system is its applicability to
334 a variety of biomolecules not only DNA and RNA but also proteins such as enzymes and antibodies
335 tagged with dextran-binding domain (DBD). We conducted the concentration-driven LIPS using the
336 Soret effect, which gave flexibility of generation temperature. Simple setup by conventional
337 equipment gave accessibility for laboratory use. Those features widen the possibility of applications
338 of LIPS droplets in biological research. The properties of encapsulating substances accompanied by
339 phase separation, are important also in pharmaceuticals[41], medical science, and agricultural science.
340

341 **Methods**

342 **Materials.** We prepared a sample by mixing Dextran (DEX, Mw = 4.5 – 6.5 × 10^5, Sigma),
343 Polyethylene glycol (PEG, Mn = 3.5 × 10^4, Aldrich), λ-DNA (48,502 bp, Nippon Gene), and pure water.
344 To visualise and evaluate the concentration of polymers, we used TRITC-Dextran (Mw = 5.0 × 10^5,
345 Sigma) and FITC-PEG (Mw = 3.0 × 10^4, Creative PEG Works). DNA was visualised using an
346 intercalator (SYBR Gold; Invitrogen). DEX and PEG were dissolved in water at 20 wt.% as stock
347 solutions before mixing.

348 The phase diagram of the system is shown in Fig. 1a. We chose the system of the above molecular
349 weights of DEX and PEG because the temperature dependence of the phase diagram is negligible. This
350 means that our droplet generation is not induced by temperature-driven phase separation but by the
351 Soret effect. We confirmed this property experimentally by the fact that phase separation cannot be
352 induced by heating the bulk sample (see also Supplementary Note 2). Note that the temperature effect
353 to phase separation in DEX/PEG system depends on the molecular weight of polymers and there are
354 other DEX/PEG systems which show clear temperature dependence for the lower molecular weight of
355 DEX and PEG[28,42].

356 For the droplet-generation experiments, we first prepared a sample with an initial composition in
357 the two-phase region to experimentally obtain a sample on the coexisting curve. All components were
358 mechanically mixed using a conventional vortex mixer and centrifuged at 15,000 rpm (Eppendorf
359 Himac Technologies, CF18RS relative centrifugal force of 16,451.37*g*) for 20 min under temperature
360 control at 298 K. The upper PEG-rich phase (indicated by an arrow in Fig. 1a) produced from the
361 mixture was extracted and used as a sample. For the mixture of DEX 2.6 wt.% PEG 6 wt.% (open
362 circle in Fig. 1a), the composition of two separated phases after centrifugation estimated from the
363 fluorescent intensity of a dye (TRITC-DEX, FITC-PEG) using a microplate reader (Molecular
364 Devices, SpectraMax iD3) was DEX 0.7 wt.% and PEG 3.1wt.% for the upper PEG-rich phase and
365 DEX 8.4 wt.% and PEG 0.9 wt.% for the lower DEX-rich phase, where we assumed that the

366 concentration of the polymer with the dye was directly proportional to that of the dye-free polymer
367 of the same type. The quantity of fluorescently labelled DEX varied from 0.02%–0.2% depending on
368 the experiment. The concentrations in the text denote the total DEX concentration. The DNA
369 concentration of each equilibrated phase was 70 pg/μL for the upper PEG-rich phase estimated by
370 the confocal image of DNA, and 60 ng/μL for the lower DEX-rich phase estimated by spectroscopy
371 (Thermo Scientific, NanoDrop 2000).
372 To observe the spontaneously forming droplets, we used a vortex mixer to agitate the solution for
373 a few minutes. Subsequently, we used the upper PEG-rich phase containing DEX-rich droplets after
374 waiting for a sufficient amount of time for sedimentation to reduce the number of droplets for 30 min.
375
376 **Local heating experiments and microscopy.** Local heating was performed under a microscope
377 (Nikon Ti2E). An infrared (IR) laser with a wavelength of 1,064 nm was connected to the microscope
378 and focused on the sample (Thorlabs; Diode laser 1064 nm, a laser power of 30 mW at the sample
379 position). The sample was sandwiched between a cover glass and a glass plate with ITO (Indium Tin
380 Oxide) coating (EHC. Co. Ltd.; ITO thickness = 20–40 nm, and resistance = 100 ohms). ITO absorbs
381 light of wavelength 1,064 nm, which causes a temperature increase at the beam position. The sample
382 thickness was controlled by a polyimide film with a thickness of 85 μm. The temperature of the
383 sample cell was controlled at 298 ± 0.1 K by a temperature stage (Linkam PE120) with a Peltier
384 module. For multiple-droplet generation, temperature control is necessary to prevent the temperature
385 gradient caused by laser irradiation from influencing the droplets. The maximum temperature increase
386 by local heating was approximately 10 K, which was estimated from the temperature dependence of
387 fluorescence intensity of Rhodamine B solution in water (Supplementary Note 1). The microscope
388 images were captured using a CMOS camera (Andor Zyla).
389 For confocal microscopy, the droplets were generated using the local heating setup described
390 above and they were observed under a confocal microscope (Leica Microsystems, SP-8). The glass

391 plate (thickness of 0.7 mm) with an ITO coating is greater than the working distance of the objective
392 lens (100X, N.A. 1.47) used in confocal microscopy. The sample cell was flipped, and the induced
393 droplets were observed from the bottom. For the simultaneous observation of induced and
394 spontaneous droplets, a glass plate (thickness 0.2 mm) with an ITO coating was used without flipping
395 over the plate. A white laser was used for excitation (488 nm for SYBR gold or FITC-PEG and 561
396 nm for TRITC-DEX), and the experiment was performed with the minimum number of acquisitions
397 to reduce the contribution of photobleaching. We did not perform 3D acquisition every time in a time-
398 course measurement and analysed kinetics using the droplet diameter instead of droplet volume for
399 the same reason. Under this condition, the decrease in intensity caused by photobleaching can be
400 considered negligible (Supplementary Note 5). The background light caused by the reflection of the
401 laser from the substrate was removed by notch filters and time-gated acquisition from 0.2 ns. The
402 time evolution was observed at room temperature (297 ± 0.5 K). The droplet diameter was estimated
403 by contour detection using commercial software (Image Pro Plus, Media Cybernetics). As the
404 obtained values could be underestimated, we set the error bar to ± 0.5 μm. For the non-linear fit
405 analysis of the droplet diameter, we added the initial droplet diameter after LIPS (t = 0) determined
406 from the phase contrast microscopy image to the time evolution of the droplet diameter observed by
407 confocal microscopy as the value d_0 at t = 0.
408 For the estimation of the composition of the LIPS droplets, we performed the LIPS droplet
409 generation experiments on the sample including fluorescently labelled DEX and PEG (TRITC-
410 Dextran (Mw = 5.0×10^5, Sigma) and FITC-PEG (Mw = 3.0×10^4, Creative PEG Works)). The
411 concentration ratios of DEX (CR^{DEX}) and PEG (CR^{PEG}) between the droplet and the surrounding phase
412 were determined as a fluorescent intensity ratio. They were converted to the concentration by
413 multiplying the concentration of the surrounding phase (0.7 wt.% for DEX, 3.1 wt.% for PEG).
414
415 **Estimation of absolute DNA concentration.** We determined the DNA concentration by comparison

with the confocal data of DNA suspension in water with SYBR gold (See also Supplementary Note 4). At a low concentration range below 100 pg/μL, DNA molecules are isolated and visible in confocal images because the full length of λ-DNA (48,502 bp) is approximately 16 μm. We counted the number of DNA molecules in several images and obtained the concentration dependence of the number per unit area (Extended Data Fig. 6). At the concentration range above 100 pg/μL, it becomes difficult to distinguish the isolated DNA molecules. We observed the confocal image of DNA suspensions in the same sample cell and other experimental conditions with that of the LIPS experiments. The concentration dependence of the average fluorescent intensity was measured and used to determine the absolute concentration of the LIPS droplets.

Acknowledgements

The authors thank Masao Doi for stimulating discussions on the mechanism of metastability. They thank Hajime Tanaka for helpful discussions on phase separation kinetics and his constant encouragement. They are grateful to Takahiro Muraoka for valuable discussions and his encouragement. They also thank Yutaro Ii for providing RNA samples, Shinichiro Kanatsuki for technical support of temperature control, and Kazutaka Irisawa for the optimization of ITO coating. This work was supported in part by Grant-in-Aid for Scientific Research (S; JP19H05624 to H.N.) and (C; 19K03763 to M.K.) from the Japan Society for the Promotion of Science (JSPS), and JST CREST, Japan (JPMJCR19S4 to H.N.), and the Kao Foundation for Arts and Sciences (Kao Crescent award to M.K.).

Author contributions

H.N. designed the project and supervised the study. M.K. performed the experiments and discovered the long-time presence of LIPS droplets. M.K. interpreted the physical mechanism underlying the phenomenon and analysed the data. All authors discussed the results. M. K. and H. N. prepared the

manuscript.

Competing interests

The authors declare no competing interests.

Correspondence and requests for materials should be addressed to Hiroyuki Noji or Mika Kobayashi.

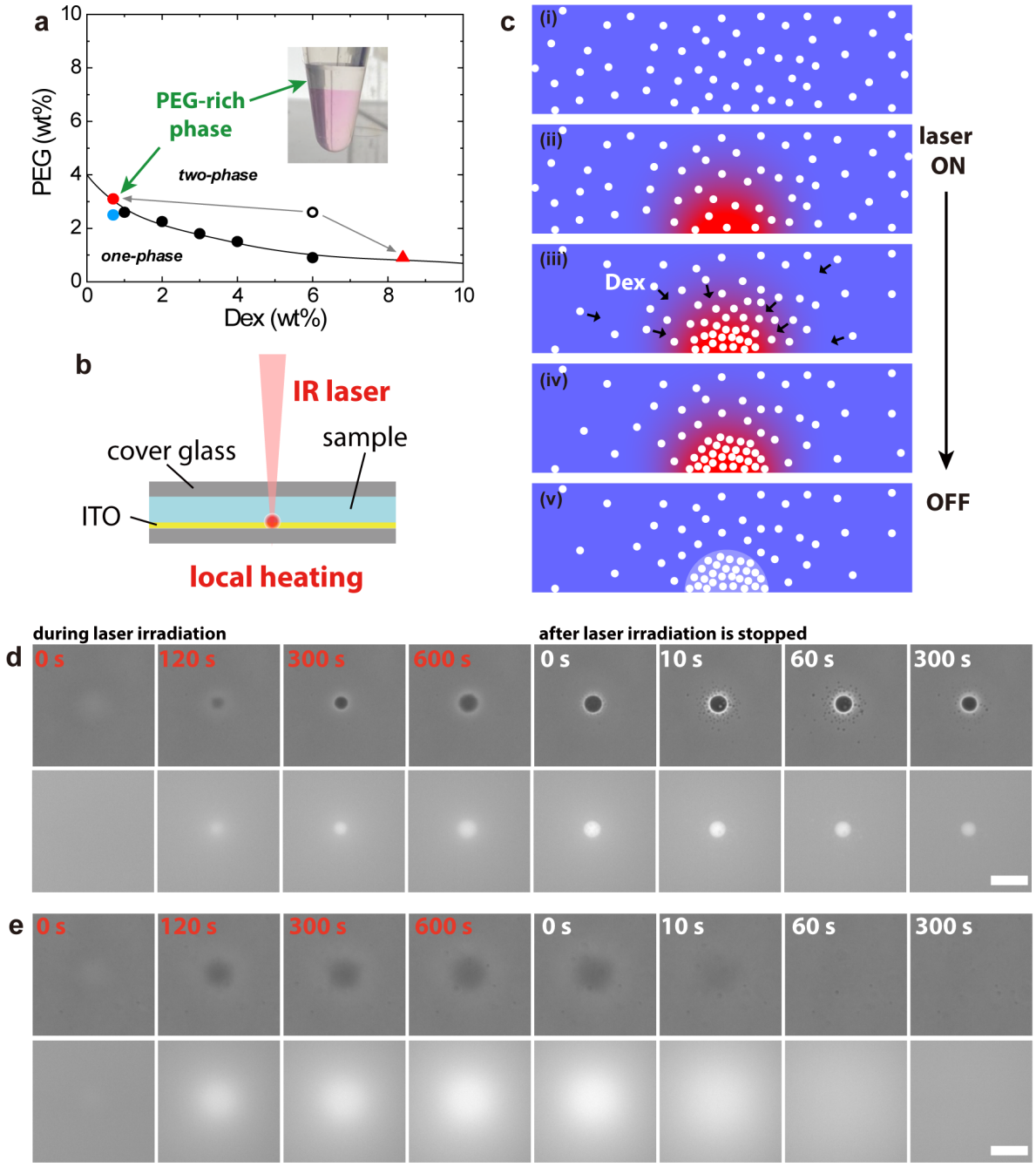

Fig. 1: Droplet generation induced by the Soret effect.

a, Phase diagram of the ATPS of Dextran (M_w = 5.5 × 10^5) and PEG (M_w = 3.5 × 10^4). The black circles are phase boundary obtained by visual observation. A sample was prepared with an initial composition of 6 wt.% and PEG 2.6wt.% (open circle) in a two-phase region. The mixture was phase-separated, and the composition of each phase is indicated by a red circle and triangle (See Methods). The upper PEG-rich phase of the phase-

separated mixture was used in droplet generation experiments. The black curve represents the coexisting curve. **b**, Experimental setup. The ITO coated on the cover glass absorbs laser light and causes local heating. **c**) Droplet generation process induced by the Soret effect. (See text.) Side view of the laser focus region. The white particles denote the dextran molecules. (i) Before laser irradiation. (ii) A temperature gradient occurs at the ITO surface when the laser irradiation is initiated. (iii) Dextran molecules enter the hot region. (iv) A dextran-rich domain formed. (v) The phase-separated droplets remain after the laser is switched off. **d**, Droplet generation process (Sample: upper phase of DEX 6 wt.% and PEG 2.6 wt.% including fluorescently labelled DEX 0.2 wt.%). (top) Phase contrast images. (Bottom) Fluorescence images of dextran. When the laser irradiation was initiated, a dark dextran-rich domain gradually appeared, and the droplet interface became sharp when the laser irradiation was stopped (see text). Successful droplet generation was observed only for the sample at the phase boundary. Scale bar = 20 μm. **e**, Cases in which no droplets were generated (DEX 0.7 wt.% and PEG 2.5 wt.% blue circle in the phase diagram). The sample composition was very close to that of **d** but only the behaviour caused by the Soret effect was observed. Dextran collected by the Soret effect diffuses rapidly after the laser is switched off (local heating is removed). (top) Phase contrast images. (Bottom) Fluorescence images of dextran. Scale bar = 20 μm.

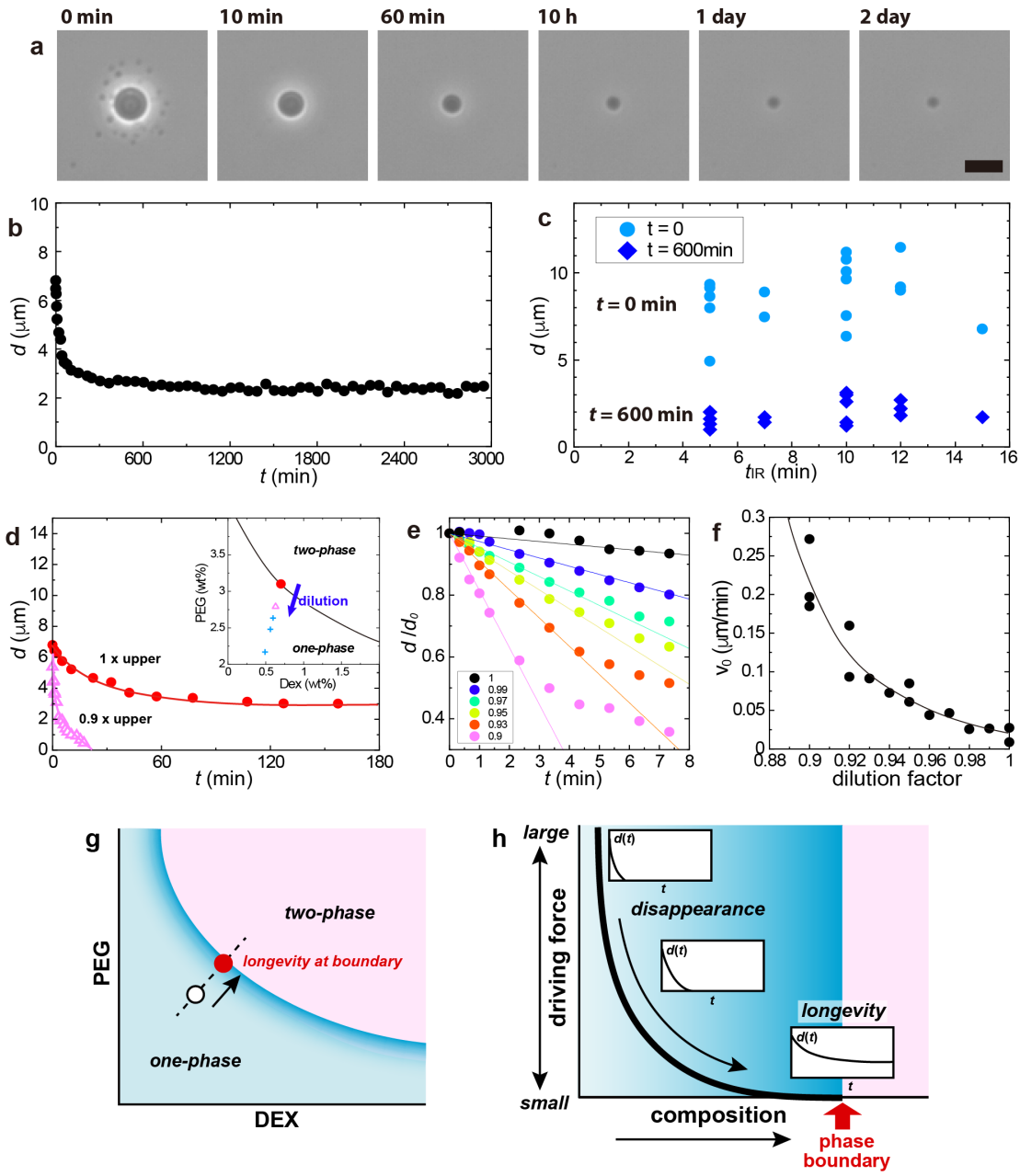

Fig. 2: Long-time droplet presence and its relationship with the distance to the coexisting curve.

a-c, Cases where the droplet generated in the sample on the coexisting curve sustains for a long time. The droplet was generated in the upper phase of 6 wt.% and PEG 2.6 wt.% (red circle in Fig. 1**a**). (**a**) Time evolution of phase-contrast images after the laser was switched off. (Laser irradiation time 10 min.) The number denotes the time elapsed after the laser was disabled. The droplets did not disappear and remained for more than two days. Scale bar = 10 μm. (**b**) Time evolution of droplet diameter. The value approached a finite value of

477 approximately 3 μm and converged. (**c**); Droplet diameters at t = 0 and 600 min plotted against the laser
478 irradiation time t_{IR}. **d-f**, Relationship between droplet generation behaviour and distance to the coexisting curve
479 obtained by dilution experiments on the upper PEG-rich phase (see text). (**d**); Time evolution of droplet
480 diameter when the generated droplet disappears (pink triangles). This was attributed to the laser irradiation
481 experiment using a sample of the diluted upper PEG-rich phase with a dilution factor of 0.9. The long-time
482 presence achieved without dilution (dilution factor 1) is plotted for comparison (red circles). The solid curves
483 are visual guides. The inset shows the schematic illustration of dilution experiments. Red circle: upper PEG-
484 rich phase: sample on the coexisting curve (solid curve). Diluting the upper PEG-rich phase increases the
485 distance from the coexisting curve (a smaller dilution factor corresponds to being more distant from the
486 coexisting curve). The condition where the produced droplet disappeared (Pink triangle: dilution factor = 0.9).
487 Further dilution makes a condition where droplet generation is unsuccessful (Blue crosses). (**e**); Droplet
488 diameter in the initial regime. The diameter is normalized by the initial value at t = 0. The lines represent the
489 linear fits of the initial linear regime of time dependence. Numbers in the legend denote the dilution factor. (**f**);
490 Initial speed of droplet shrinkage obtained as the slope in the fit results in **e**. The speed decreases approaching
491 the coexisting curve: dilution factor =1. The solid curves represent visual guides. **g,h**, Schematic illustration
492 of the mechanism of longevity. (**g**); Schematic phase diagram of a DEX/PEG system. LIPS droplets generated
493 from the open circle inside the one-phase region disappear. When the initial sample is on the phase boundary
494 (red circle), LIPS droplet exhibits longevity. (**h**); The relationship between the behaviour of a LIPS droplet
495 (time dependence of droplet diameter d(t) after switching off the laser) and the initial composition of the sample.
496 The longevity appears when the initial composition is approaching the phase boundary because of decreasing
497 the driving force to make the created LIPS droplet disappear.

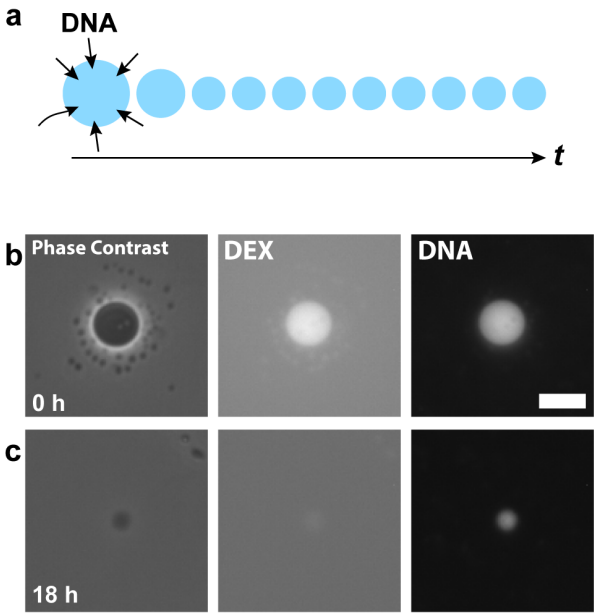

Fig. 3: DNA enrichment in the LIPS droplet.

a, Schematic illustration of the concept of long-time DNA enrichment in LIPS droplets. **b, c**, The droplet was induced by laser irradiation for 5 min to the upper PEG-rich phase of DEX 6 wt.% and PEG 2.6wt.% + λ-DNA (48,502 bp) 29 ng/μL. **b**, t = 0 h; **c**, t = 18 h after the laser is disabled. Phase-contrast image, fluorescent image of dextran, and fluorescent image of the DNA observed by epifluorescence microscopy from left to right. The droplet was visualised using a DNA intercalator and fluorescently labelled dextran. The DNA was successfully incorporated into the generated dextran-rich droplet. Scale bar = 10 μm.

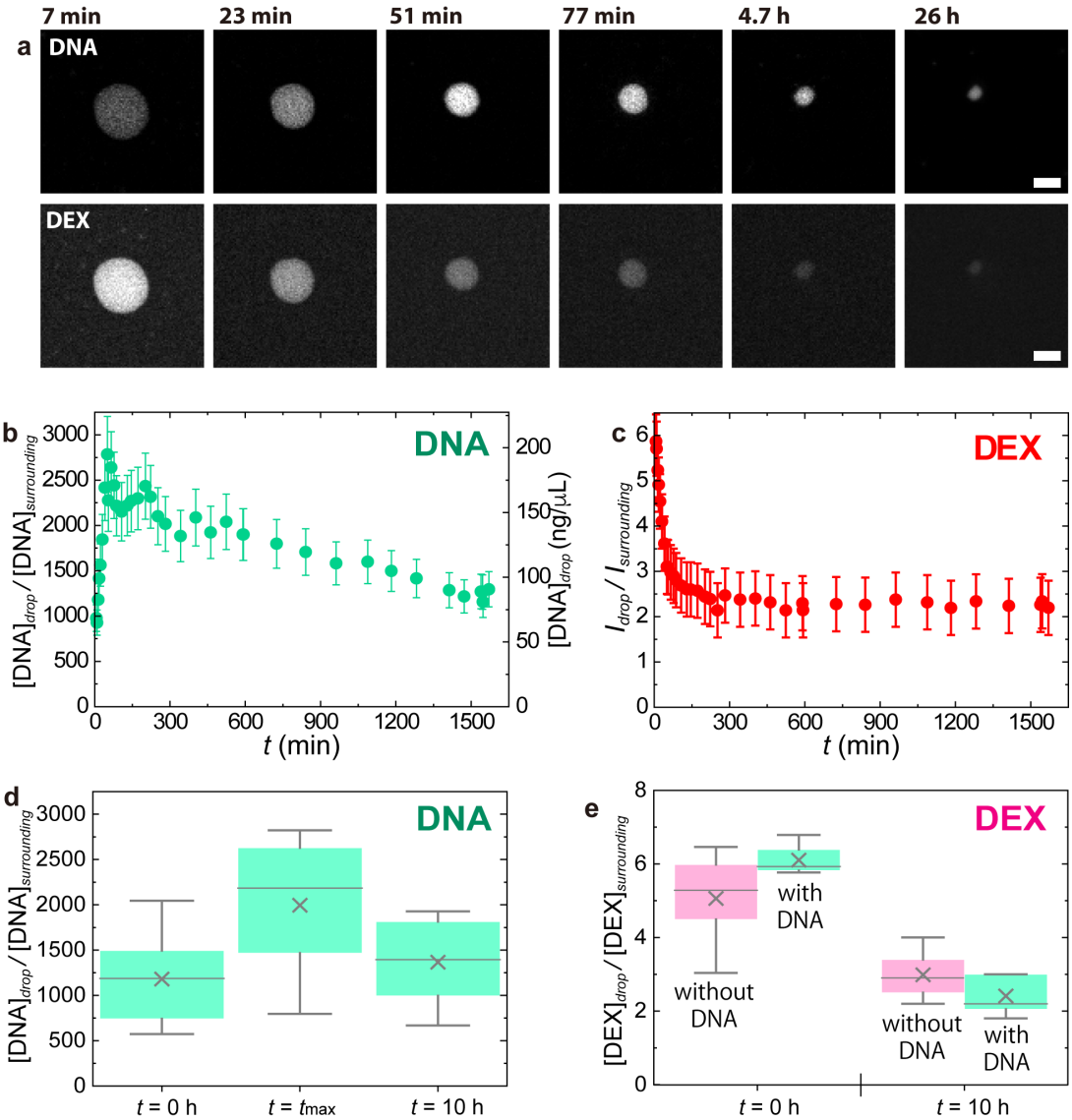

506

507 **Fig. 4: Time evolution of LIPS droplet observed by confocal measurements.**

508 The droplet was generated by laser irradiation for 12 min to the upper PEG-rich phase of DEX 6 wt.% and

509 PEG 2.6 wt.% + λ-DNA (48,502 bp) 29 ng/μL. **a,** Time-lapse image of a droplet visualised using a DNA

510 intercalator and fluorescently labelled dextran. The time in each image is the time after the termination of the

511 laser. Scale bar = 5 μm. **b**, DNA enrichment factor. Error bars are estimated from standard deviation in the

estimation of $c_{\mathrm{surrounding}}$. **c**, Fluorescence intensity ratio of dextran. Error bars represent uncertainties from focal positions. **d**, DNA enrichment factor at characteristic times. The time t_{max} denotes the time when the DNA enrichment factor reaches its maximum value. It depends on the experiment (51 min for Fig. 4b) and is shown in Extended Data Fig. 3. **e**, Dex intensity ratio at characteristic times in the case with and without DNA. In **d** and **e**, 25–75 percentile (box), median (line), mean (cross), highest/lowest observations (whiskers).

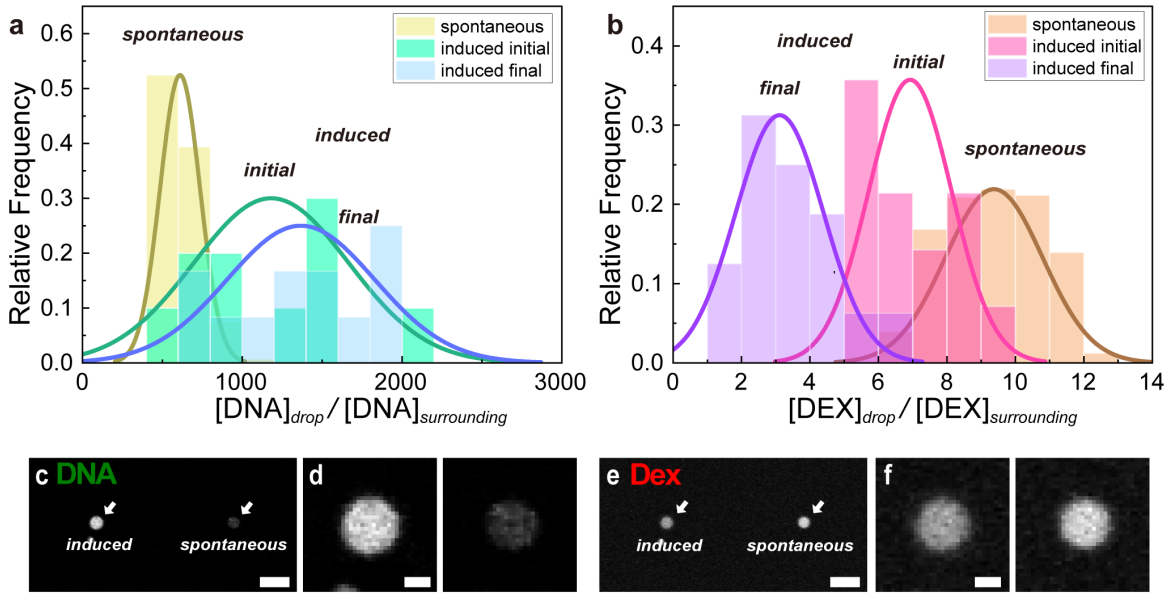

528 **Fig. 5: Comparison between LIPS droplets and the droplets by spontaneous phase separation. a-b**,
529 Histogram of the DNA enrichment factor and DEX concentration ratio of LIPS droplets and spontaneous
530 droplets. The initial ($t = 0$ h) and the final (long-time) values for LIPS droplets are displayed. The LIPS droplets
531 were generated from the upper PEG-rich phase of DEX 6 wt.% and PEG 2.6 wt.% with DNA (λ-DNA (48,502
532 bp) 29 ng/μL). Spontaneous droplets were produced from a two-phase mixture that has the same composition
533 as the one used for the preparation of the upper PEG-rich phase for LIPS experiments. **(a)**; Histogram of the
534 DNA enrichment factor. **(b)**; Histogram of concentration ratio of DEX between the droplet and the surrounding
535 phase. **c-f**, Confocal images of a LIPS droplet generated by laser irradiation for 7 min and a droplet generated
536 by spontaneous phase separation. The droplets were observed at t = 7 min after switching off the laser. **(c)**;
537 Confocal images of DNA. (left) LIPS droplet. (right) Droplet obtained by spontaneous phase separation. Scale
538 bar = 10 μm. **(d)**; Magnified image of droplets in Fig. 5c. Scale bar = 2 μm. **e**, Confocal image of DEX. Scale
539 bar = 10 μm. **(f)**; Magnified image of droplets in Fig. 5e. Scale bar = 2 μm.

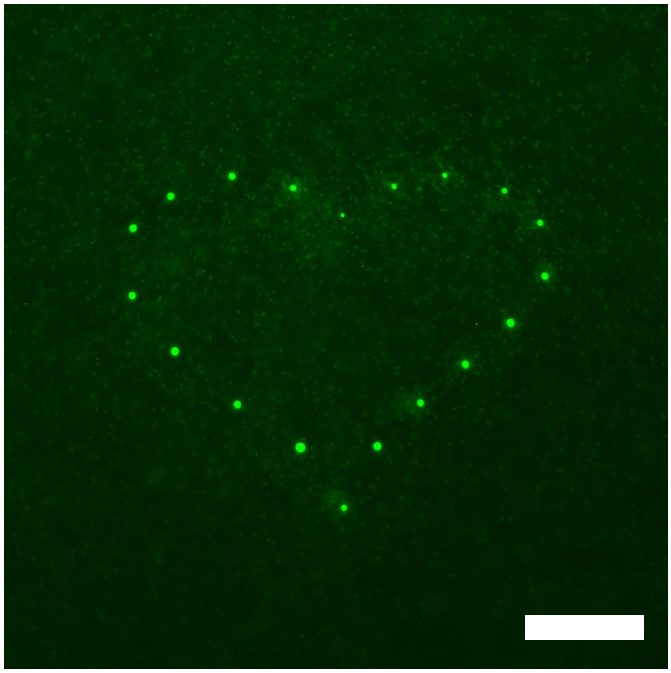

Fig. 6: Heart shape patterned by DNA-enriched droplets. Fluorescent image of λ-DNA (48,502 bp) observed by epifluorescence microscopy. Each droplet was generated by the laser irradiation of the sample for 5 min to the upper PEG-rich phase of DEX 6 wt.% and PEG 2.6 wt.% + λ-DNA (48,502 bp) 29 ng/μL. Scale bar = 100 μm.

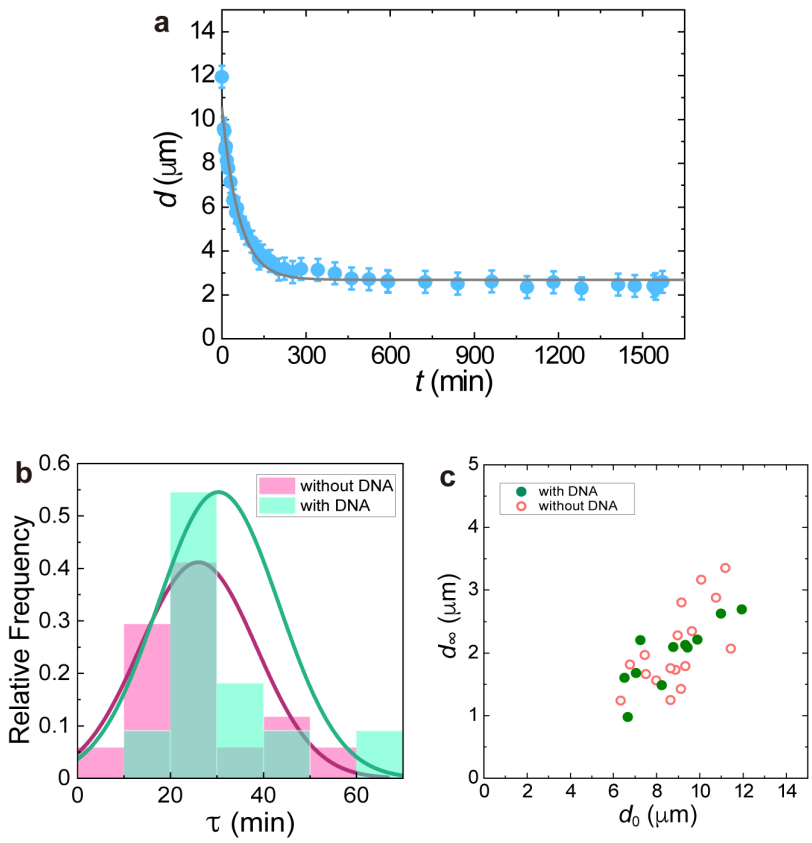

Extended Data Fig. 1: Time evolution of droplet diameter. a, Time evolution of the droplet diameter for the same experiment shown in Fig. 4a-c. The droplet was generated by laser irradiation for 12 min to the upper PEG-rich phase of DEX 6 wt.% and PEG 2.6 wt.% + λ-DNA (48,502 bp) 29 ng/μL. The value at $t = 0$ was obtained from the phase-contrast image. The rest were obtained from the confocal images of DNA. The diameter approaches a finite value. The solid curve was obtained by fiting the data to a function, $d(t) = (d_0 - d_\infty) \exp(-t/\tau) + d_\infty$, where d_0 and d_∞ represent the diameters at $t = 0$ and $t = \infty$, respectively, and τ represents the characteristic decay time. The fitting parameters from the fit were τ = 60.7 min and d_∞= 2.7 μm. **b**, Histogram of the decay time of droplet diameter in the case with and without DNA. **c**, Final droplet diameter d_∞ at $t = \infty$ estimated by the fit plotted against the initial droplet diameter d_0 at $t = 0$ (measured from phase

contrast image). Green circles: cases with DNA. Red open circles: without DNA. The droplets were generated from the upper PEG-rich phase of DEX 6 wt.% and PEG 2.6 wt.% with/without DNA (λ-DNA (48,502 bp) 29 ng/μL)).

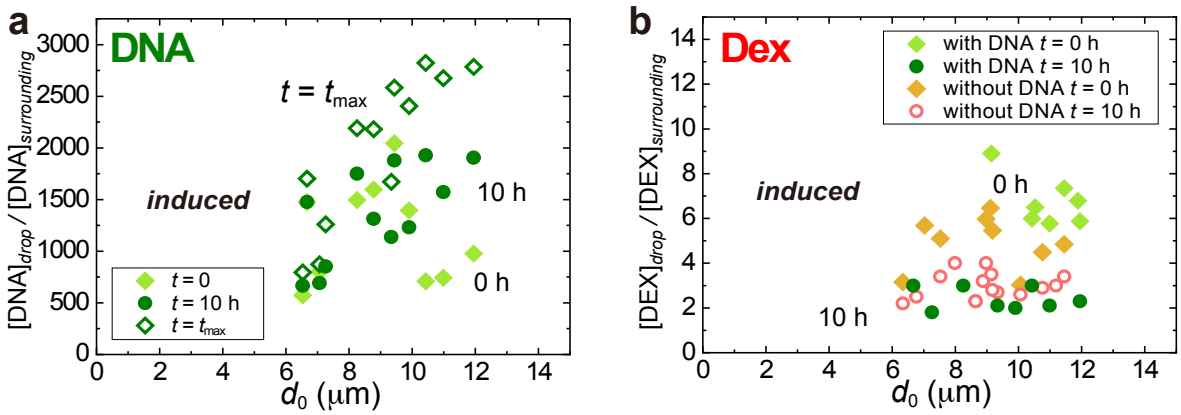

578

579 **Extended Data Fig. 2: The DNA enrichment factor and DEX concentration ratio. a**, The DNA enrichment

580 factor of LIPS droplets. The initial value (t = 0 h), maximum value ($t = t_{max}$), and long-time value (t = 10 h).

581 The droplets were generated from the upper PEG-rich phase of DEX 6 wt.% and PEG 2.6 wt.% with DNA (λ-

582 DNA (48,502 bp) 29 ng/μL). **b**, Concentration ratio of DEX between the droplet and surrounding phase of the

583 induced droplets at t = 0, 10 h estimated from the fluorescence intensity ratio of dextran. The droplets were

584 generated from the upper PEG-rich phase with/without DNA (DEX 6 wt.% and PEG 2.6 wt.% with/without

585 DNA (λ-DNA (48,502 bp) 29 ng/μL).

586

587

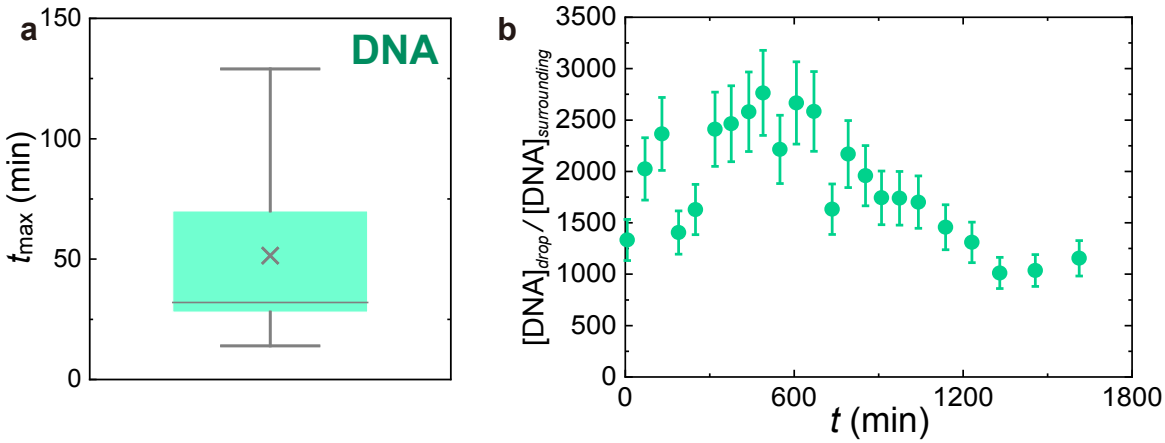

Extended Data Fig. 3: Behaviour of DNA enrichment factor to reach its maximum value. a, Time scale when the enrichment factor of DNA (EF^{DNA}) reached its maximum value. 25–75 percentile (box), median (line), mean (cross), highest/lowest observations without outliers (whiskers). **b,** A case where EF^{DNA} showed a broad time change and showed its maximum value at a very long time around 500 min. The factor EF^{DNA} was kept at a high value of more than 2500 for an exceedingly long time.

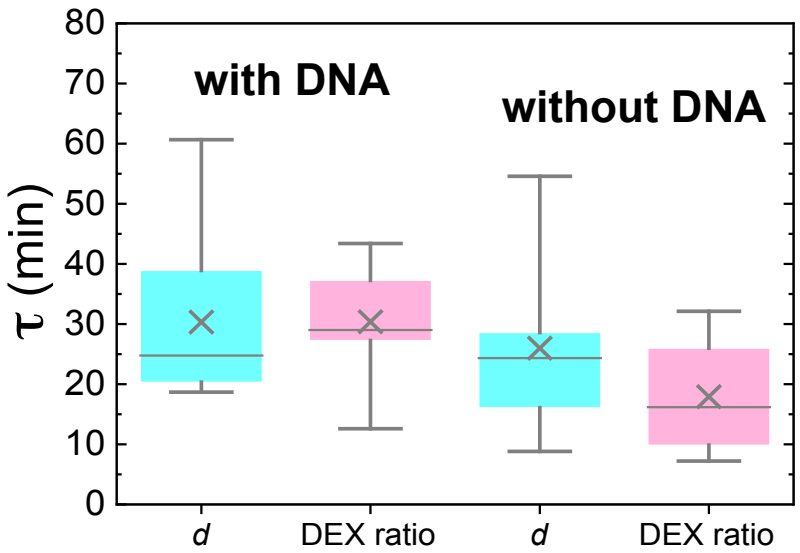

Extended Data Fig. 4: Comparison of timescale between the droplet shrinkage and the DEX concentration change. Decay time was estimated by exponential fit. The function used for the fit was the same expression as that given in Extended Data Fig. 1. Decay time of droplet diameter (light blue) and DEX concentration ratio (pink) in the case of w/ and w/o DNA. 25–75 percentile (box), median (line), mean (cross), highest/lowest observations (whiskers).

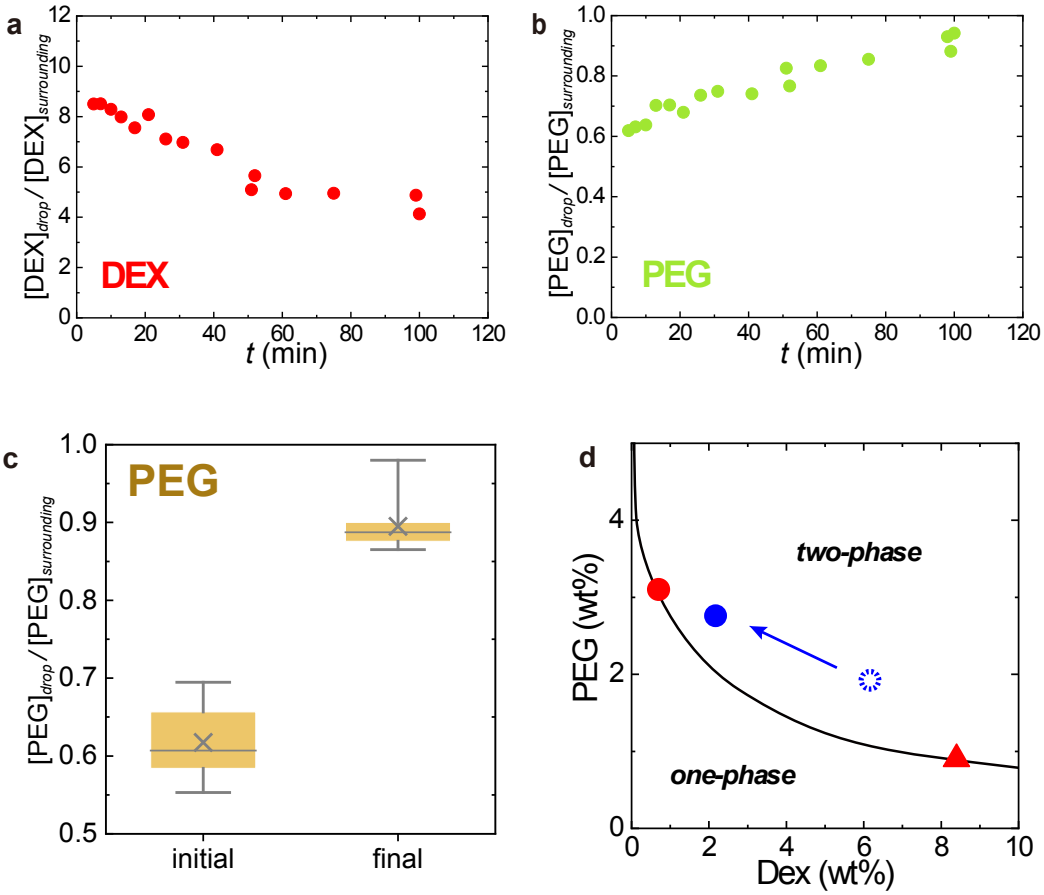

615

616 **Extended Data Fig. 5: Observation of the composition of LIPS droplets. a-b**, Typical time evolution of (**a**)

617 DEX and (**b**) PEG concentration ratios of a LIPS droplet. The droplet was generated by laser irradiation for

618 11 min to the upper PEG-rich phase of DEX 6 wt.% and PEG 2.6 wt.% + λ-DNA (48,502 bp) 29 ng/μL

619 (including 0.2 wt% of TRITC-Dextran and FITC-PEG). The concentration ratios of DEX and PEG were

620 estimated from the fluorescent intensity of dye (TRITC-DEX and FITC-PEG) in confocal measurements. **c**,

621 PEG concentration ratio. 25–75 percentile (box), median (line), mean (cross), highest/lowest observations

622 (whiskers). Data w/ and w/o DNA are both included because there was no clear difference beyond experimental

error. **d**, The final composition of the LIPS droplets in a metastable state which is shown in the phase diagram. The final composition (closed blue circle) was estimated from the long-time value of DEX and PEG concentration ratio of the LIPS droplet by confocal measurements. The composition just after generation (at around t = 5 min) is indicated by a dotted circle. Red circle: upper PEG-rich phase used for LIPS experiment, red triangle: lower DEX-rich phase. The solid curve is the coexisting curve. The composition changed with time approaching the original upper phase and stopped at the blue circle.

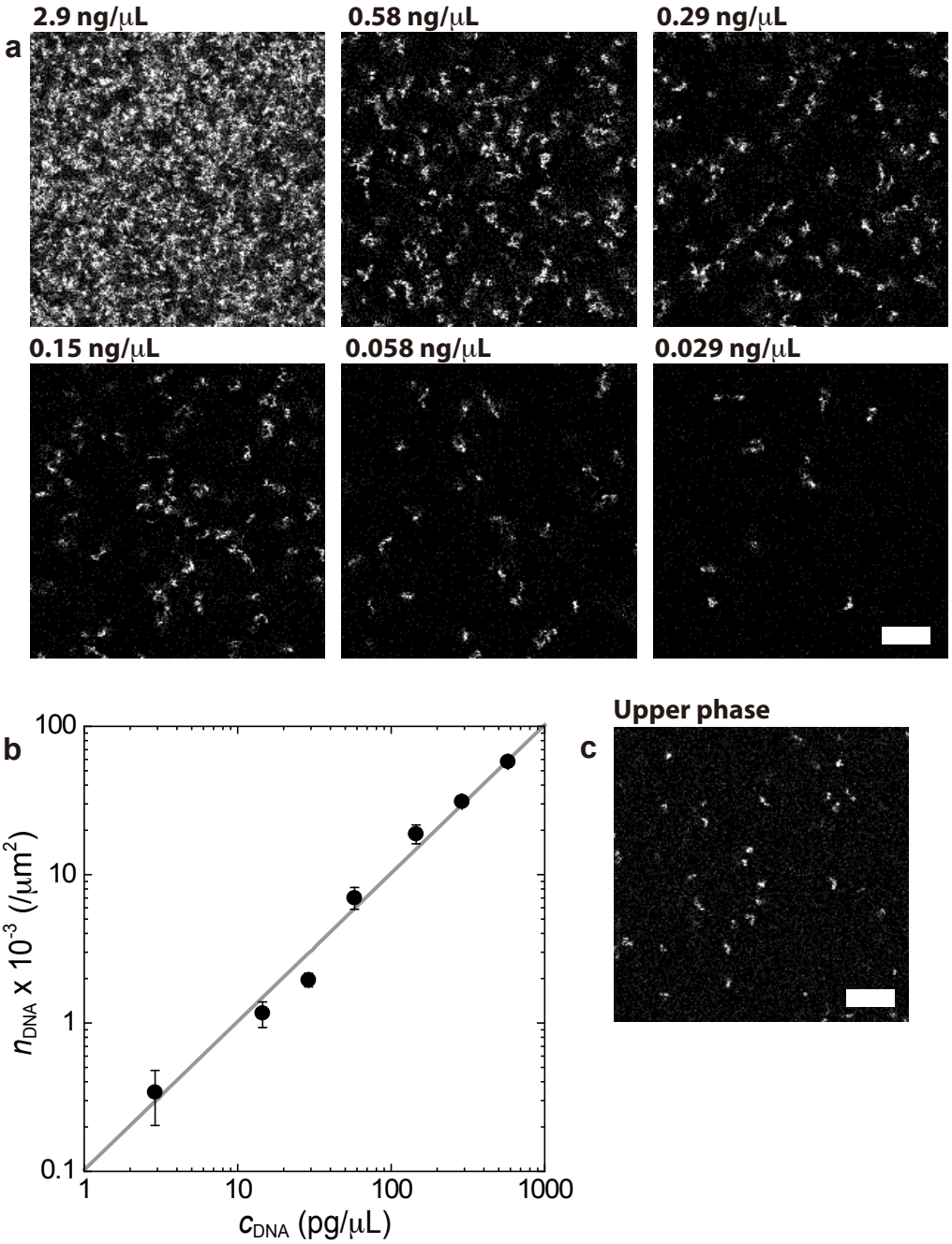

Extended Data Fig. 6: Confocal images of DNA suspensions. a, DNA suspension in water at several concentrations, λ-DNA (48,502 bp) visualised using DNA intercalator (SYBR gold). These samples were observed in a sample cell made of two coverslips with an 85-μm-thick spacer. The experiments were performed

633 at room temperature (297 ± 0.5 K). Scale bar = 10 μm. **b**, Number of DNA molecules per unit area as a function

634 of DNA concentration observed in DNA suspensions in water. Error bars are the standard deviation of at least

635 10 images. The solid line is a linear fit of the data. **c**, Upper PEG-rich phase prepared at total composition:

636 DEX 6 wt.% and PEG 2.6wt.% + λ-DNA (48,502 bp) 29 ng/μL). Scale bar = 10 μm.

637

638

639

640

641

642

643

644

645

646

647

648

649

650

651

652

653

References

1. Hyman, A. A., Weber, C. A. & Jülicher, F. Liquid-Liquid Phase Separation in Biology. *Annu Rev Cell Dev Bi* **30**, 39–58 (2014).

2. Shin, Y. & Brangwynne, C. P. Liquid phase condensation in cell physiology and disease. *Science* **357**, eaaf4382 (2017).

3. Alberti, S., Gladfelter, A. & Mittag, T. Considerations and Challenges in Studying Liquid-Liquid Phase Separation and Biomolecular Condensates. *Cell* **176**, 419–434 (2019).

4. Dignon, G. L., Best, R. B. & Mittal, J. Biomolecular Phase Separation: From Molecular Driving Forces to Macroscopic Properties. *Annu Rev Phys Chem* **71**, 53–75 (2020).

5. Albertsson, P.-Å. Partition of Proteins in Liquid Polymer–Polymer Two-Phase Systems. *Nature* **182**, 709–711 (1958).

6. Crowe, C. D. & Keating, C. D. Liquid–liquid phase separation in artificial cells. *Interface Focus* **8**, 20180032 (2018).

7. Sakuta, H. *et al.* Aqueous/Aqueous Micro Phase Separation: Construction of an Artificial Model of Cellular Assembly. *Front Chem* **7**, 44 (2019).

8. Minagawa, Y., Nakata, S., Date, M., Ii, Y. & Noji, H. On-Chip Enrichment System for Digital Bioassay Based on Aqueous Two-Phase System. *Acs Nano* **17**, 212–220 (2023).

9. Nakatani, N. *et al.* Specific Spatial Localization of Actin and DNA in a Water/Water Microdroplet: Self-Emergence of a Cell-Like Structure. *Chembiochem* **19**, 1370–1374 (2018).

10. Shanbhag, V. P. & Axelsson, C. Hydrophobic Interaction Determined by Partition in Aqueous Two-Phase Systems. *Eur J Biochem* **60**, 17–22 (1975).

11. Chao, Y. & Shum, H. C. Emerging aqueous two-phase systems: from fundamentals of interfaces to biomedical applications. *Chem Soc Rev* **49**, 114–142 (2020).

12. Frampton, J. P. *et al.* Aqueous two-phase system patterning of detection antibody solutions for cross-reaction-free multiplex ELISA. *Sci. Rep.* **4**, 4878 (2014).

680 13. Ma, Q. *et al.* Cell-Inspired All-Aqueous Microfluidics: From Intracellular Liquid–Liquid Phase
681 Separation toward Advanced Biomaterials. *Adv. Sci.* **7**, 1903359 (2020).

682 14. Xu, Z. *et al.* Photosynthetic hydrogen production by droplet-based microbial micro-reactors under
683 aerobic conditions. *Nat. Commun.* **11**, 5985 (2020).

684 15. Mizuuchi, R. & Ichihashi, N. Translation-coupled RNA replication and parasitic replicators in
685 membrane-free compartments. *Chem. Commun.* **56**, 13453–13456 (2020).

686 16. Delville, J. P., Lalaude, C., Freysz, E. & Ducasse, A. Phase separation and droplet nucleation induced by
687 an optical piston. *Phys Rev E* **49**, 4145–4148 (1994).

688 17. Delville, J. P., Lalaude, C. & Ducasse, A. Kinetics of laser-driven phase separation induced by a tightly
689 focused wave in binary liquid mixtures. *Physica A Statistical Mech Appl* **262**, 40–68 (1999).

690 18. Mukai, S.-A., Magome, N., Kitahata, H. & Yoshikawa, K. Liquid/liquid dynamic phase separation
691 induced by a focused laser. *Appl Phys Lett* **83**, 2557–2559 (2003).

692 19. Kitamura, N., Yamada, M., Ishizaka, S. & Konno, K. Laser-Induced Liquid-to-Droplet Extraction of
693 Chlorophenol: Photothermal Phase Separation of Aqueous Triethylamine Solutions. *Anal Chem* **77**, 6055–
694 6061 (2005).

695 20. Tsuboi, Y., Nishino, M., Matsuo, Y., Ijiro, K. & Kitamura, N. Phase Separation of Aqueous Poly(vinyl
696 methyl ether) Solutions Induced by the Photon Pressure of a Focused Near-Infrared Laser Beam. *B Chem*
697 *Soc Jpn* **80**, 1926–1931 (2007).

698 21. Voit, A., Krekhov, A., Enge, W., Kramer, L. & Köhler, W. Thermal Patterning of a Critical Polymer
699 Blend. *Phys Rev Lett* **94**, 214501 (2005).

700 22. Voit, A., Krekhov, A. & Köhler, W. Laser-induced structures in a polymer blend in the vicinity of the
701 phase boundary. *Phys Rev E* **76**, 011808 (2007).

702 23. Shimizu, M. *et al.* Space-selective phase separation inside a glass by controlling compositional
703 distribution with femtosecond-laser irradiation. *Appl Phys* **100**, 1001–1005 (2010).

704 24. Yuyama, K., Sugiyama, T. & Masuhara, H. Millimeter-Scale Dense Liquid Droplet Formation and
705 Crystallization in Glycine Solution Induced by Photon Pressure. *J Phys Chem Lett* **1**, 1321–1325 (2010).

706 25. Walton, F. & Wynne, K. Control over phase separation and nucleation using a laser-tweezing potential.
707 *Nat Chem* **10**, 506–510 (2018).

26. Walton, F. & Wynne, K. Using optical tweezing to control phase separation and nucleation near a liquid–liquid critical point. *Soft Matter* **15**, 8279–8289 (2019).

27. Gowayed, O. Y. *et al.* Dynamic Light Scattering Study of a Laser-Induced Phase-Separated Droplet of Aqueous Glycine. *J Phys Chem B* **125**, 7828–7839 (2021).

28. Pavlovic, M., Antonietti, M., Schmidt, B. V. K. J. & Zeininger, L. Responsive Janus and Cerberus emulsions via temperature-induced phase separation in aqueous polymer mixtures. *J Colloid Interf Sci* **575**, 88–95 (2020).

29. Platten, J. K. The Soret Effect: A Review of Recent Experimental Results. *J Appl Mech* **73**, 5–15 (2006).

30. Niether, D. & Wiegand, S. Thermophoresis of biological and biocompatible compounds in aqueous solution. *J Phys Condens Matter* **31**, 503003 (2019).

31. Sugaya, R., Wolf, B. A. & Kita, R. Thermal Diffusion of Dextran in Aqueous Solutions in the Absence and the Presence of Urea. *Biomacromolecules* **7**, 435–440 (2006).

32. Atefi, E., Fyffe, D., Kaylan, K. B. & Tavana, H. Characterization of Aqueous Two-Phase Systems from Volume and Density Measurements. *J Chem Eng Data* **61**, 1531–1539 (2016).

33. Maeda, Y. T., Buguin, A. & Libchaber, A. Thermal Separation: Interplay between the Soret Effect and Entropic Force Gradient. *Phys Rev Lett* **107**, 038301 (2011).

34. Maeda, Y. T., Tlusty, T. & Libchaber, A. Effects of long DNA folding and small RNA stem–loop in thermophoresis. *Proc National Acad Sci* **109**, 17972–17977 (2012).

35. Braun, D. & Libchaber, A. Trapping of DNA by Thermophoretic Depletion and Convection. *Phys. Rev. Lett.* **89**, 188103 (2002).

36. Chen, X. *et al.* Optothermally Programmable Liquids with Spatiotemporal Precision and Functional Complexity. *Adv. Mater.* **34**, e2205563 (2022).

37. Onuki, A. *Phase Transition Dynamics*. (Cambridge University Press, 2002).

38. Brangwynne, C. P. *et al.* Germline P Granules Are Liquid Droplets That Localize by Controlled Dissolution/Condensation. *Science* **324**, 1729–1732 (2009).

39. Hnisz, D., Shrinivas, K., Young, R. A., Chakraborty, A. K. & Sharp, P. A. A Phase Separation Model for Transcriptional Control. *Cell* **169**, 13–23 (2017).

735 40. Boeynaems, S. *et al.* Protein Phase Separation: A New Phase in Cell Biology. *Trends Cell Biol* **28**, 420–
736 435 (2018).

737 41. Iwata, T. *et al.* Liquid Droplet Formation and Facile Cytosolic Translocation of IgG in the Presence of
738 Attenuated Cationic Amphiphilic Lytic Peptides. *Angew. Chem. Int. Ed.* **60**, 19804–19812 (2021).

739 42. Helfrich, M. R., Mangeney-Slavin, L. K., Long, M. S., Djoko, K. Y. & Keating, C. D. Aqueous Phase
740 Separation in Giant Vesicles. *J Am Chem Soc* **124**, 13374–13375 (2002).

741